Geophys. J. Int. (2005) **163,** 403–418 doi: 10.1111/j.1365-246X.2005.02730.x

Inverse modelling of volcanomagnetic fields using a genetic algorithm technique

Gilda Currenti,[1] Ciro Del Negro[1] and Giuseppe Nunnari[2]

[1] *Istituto Nazionale di Geofisica e Vulcanologia, Sezione di Catania, Italy. E-mail: currenti@ct.ingv.it*
[2] *Dipartimento di Ingegneria Elettrica, Elettronica e dei Sistemi, Università di Catania, Italy*

Accepted 2005 June 28. Received 2005 May 23; in original form 2004 November 19

SUMMARY

The inversion problem deals with the identification of the parameters of a volcanic source that causes observable changes in magnetic data recorded in volcanic areas. To study the inverse problem, synthetic data were generated by considering different volcanic sources: the traditional Mogi model, used for describing the inflation/deflation of the magma reservoir, and the Okada source that seems more realistic to model the opening of eruptive fractures. The main geophysical mechanisms leading to magnetic anomalies in volcanically active areas were considered, such as thermomagnetic, piezomagnetic and electrokinetic effects. The inversion problem was formulated following an optimization approach based on the use of genetic algorithms. Firstly, a number of tests were carried out on synthetically generated data to assess the performance of the inversion procedure. An appropriate index was defined to statistically evaluate the accuracy for each parameter of the sources. The results obtained show that both the Mogi and Okada models can be inverted unambiguously provided that a sufficient number of measuring points are considered. Secondly, two real case studies, concerning the thermomagnetic anomaly observed during the 1989 Mt Etna eruption and the piezomagnetic field detected during the 2000 Miyakejima volcano eruption, are reported together with their sensitivity analyses of the inverse solutions obtained. Application of the GA technique to data taken on Mt Etna and Miyakejima volcano allows for estimating the optimum parameters of volcanomagnetic sources.

Key words: genetic algorithms, inverse problem, magnetic anomalies, volcanic activity.

1 INTRODUCTION

A great variety of geophysical processes related to volcanic activity can affect the variations in the local magnetic field. Volcanoes are a kind of heat-transfer system from the depths to the ground surface, and hence, their activity is frequently accompanied by subsurface hydrothermal convection, which causes changes in temperature, pressure and fluid motion within the edifice. The modifications within the volcanic edifice of the stress field and/or of the thermodynamic state induce variations in the magnetization of the rocks, which generate a wide variety of magnetic signals (Johnston 1989). The correct identification and interpretation of these signals can be a useful instrument both for improving the monitoring of active volcanoes as well as developing a better understanding of the pre-eruptive mechanisms which produce them. The main geophysical mechanisms leading to magnetic anomalies in volcanically active areas are principally due to:

(1) piezomagnetic processes related to stress-induced changes in rock magnetization,

(2) electrokinetic effects arising from fluid flow within the volcano edifice in the presence of an electric double layer at the solid–liquid interface and

(3) thermal demagnetization or remagnetization phenomena. Usually all of these processes can produce detectable variations in the local magnetic field and it is not simple to discriminate among them. Nevertheless, the amplitude and the temporal scale of the magnetic anomaly together with other geological and geophysical evidences can guide to highlight which is the physical mechanism leading to the anomaly.

Attempts at modelling magnetic fields expected to accompany volcanic eruptions often involve a great deal of effort due to the complexity of the considered problem. Indeed, investigations on the analytical solutions for these volcanomagnetic fields, have revealed that the magnetic models are highly non-linear and, usually, characterized by many parameters. Hence, elaborated algorithms for computing such models have to be implemented to efficiently identify the source parameters.

The goal of inverse modelling is to find out as much as possible about the source parameters from the observations. A common method is manual calibration by a 'trial and error' procedure by comparing computed values from theoretical models with those measured on the field. The main drawbacks of this method are the high computational times and the difficulty in evaluating how the model parameters are to be tuned to match the measured data well.

Furthermore, this method is rather subjective, and the uncertainty on the obtained solution cannot be quantified in a rigorous way. Consequently, it cannot guarantee that the best solution is found. More structured inverse methods combine forward models with appropriate optimization algorithms to automatically find the best parameter set that minimizes an objective function (Tiampo *et al.* 2000; Jousset *et al.* 2003). Generally, these procedures search for the best set of parameters in an iterative way, by varying the parameters and combining the observed data on the field with the numerical solution provided by the model. Indeed, the search should consist of finding the global minimum of an objective function relayed on the difference between measured and computed values. The success of each method depends on the capability to reach this global minimum. For highly nonlinear models such as the volcanomagnetic fields, this is a challenging task, since the objective function can exhibit multiple local minima.

We investigate the applications of an inversion procedure based on genetic algorithms (GAs) for the estimation of the volcanomagnetic source parameters from magnetic anomaly data recorded at the ground surface. Among others, the GAs are considered due to their capability of performing a much broader search over the model parameters with a greater likelihood of finding the global optimal solution even in presence of local minima in the objective function (Goldberg 1989). Moreover, it should be remarked that an analytical proof of the uniqueness of the inverse solution for volcanomagnetic models does not exist. Hence, we carefully analyse the inversion problem for common volcanic sources in a variety of measuring scenarios in order to gain insight into the uniqueness of the inverse solutions. Further, the suitability of the inversion modelling technique was tested on field data sets. We report results obtained on two real case studies concerning the 1989 Mt Etna eruption and the 2000 Miyakejima volcano eruption.

2 VOLCANOMAGNETIC PHENOMENA

Generally speaking, volcanomagnetic fields rely upon three main endogenous causes, which are sometimes closely linked to each other in real fields. The first is that uprising melt may heat the superficial rocks to a temperature above the Curie point, with a consequent decrease in the intensity of the total field. Due to the thermal inertia of the rocks and the generally small dimensions of magmatic intrusions at shallow depths, this phenomenon is probably (1) slow and (2) restricted to a limited area. The other two causes of volcanomagnetic transients bring into play the piezomagnetism of rocks and streaming potentials. The ascent of magma to the Earth's surface will also cause the redistribution of the stress field at a shallow depth. Variation in the stress field may modify not only the magnetization of rocks but also the net of interconnected pores. Finally, circulation of groundwater driven by thermal energy will plausibly take place in dilated areas. The interstitial pressure gradients can generate electrofiltration currents, which cause the electrokinetic magnetic anomalies. Anomalies of this type show modest maximum values, but they are fast, with respect to thermomagnetic changes. Thus, volcanomagnetic signals could provide various kinds of information to understand the thermal condition, stress or pressure distribution and flow of pore fluids that are directly related to the volcanic activity.

Over the last decade, magnetic data have received increasing interest in volcano monitoring because they not only allowed the timing of the intrusive events to be described in greater detail but also, together with other volcanological and geophysical evidences, permitted some constraints to be set on the characteristics of propagation of shallow dikes (Del Negro *et al.* 2004). The comprehension of the different mechanisms, which can be the cause of volcanomagnetic signals, has advanced considerably since first observations of the phenomena. Several theoretical studies for different volcanomagnetic fields were elaborated. We have implemented some of these solutions in a unified procedure called VMM (volcanomagnetic modeling). Access to the VMM tool is possible also via Internet at the Web site: http://maglab.ct.ingv.it. It basically consists of three modules for computation of magnetic fields associated with spherical and rectangular sources.

2.1 Piezomagnetic processes

The main frame of the piezomagnetic modelling was established by Stacey (1964) and Stacey *et al.* (1965), who demonstrated the seismomagnetic and volcanomagnetic effects using the volume element method. The linear relationships established by Stacey (1964) to hold between applied stress and magnetization changes ΔJ, were reduced by Sasai (1980) to the following simple formula:

$$\Delta J = \frac{3}{2}\beta T' J, \tag{1}$$

where β is the stress sensitivity, T' is the deviatoric stress tensor, which is related to the stress tensor T and to the average stress σ_0 as:

$$T = \sigma_0 + T', \tag{2}$$

where $\sigma_0 = (\tau_{xx} + \tau_{yy} + \tau_{zz})/3$.

Schematically, the stress field is decomposed into a hydrostatic and a deviatoric component. The piezomagnetic effect would derive from the latter, provided that the temperature of the embedding rocks is below the Curie point. Prior to an eruption, it is expected that magmatic activity may lead to increase the deviatoric stress, and to the consequent increase of the local magnetic field: whereas the stress release occurring during an eruption would produce a decrease of the magnetic field (Parkinson 1983). The piezomagnetic field (B_{VP}) at the ground surface of a volcano can be estimated by (Zlotnicki & Le Mouel 1988):

$$B_{V_p}(Q,t) = -\frac{\mu_0}{4\pi}\nabla \iiint_{V_p} \frac{\Delta J(M,t)}{r^3}\, dV_M, \tag{3}$$

where μ_0 is the magnetic permeability in the vacuum, Q is the observation point, M is a point in the rock volume V_p submitted to a stress field, and r is the distance between M and Q. Application of this formula requires estimating the value of three parameters. The intensity of the piezomagnetic effect is proportional to the product of the stress sensitivity (β), the average magnetization (J) and the average rigidity of the Earth's crust (λ).

A series of theoretical studies elaborated by Sasai (1980); Sasai (1991a,b) allow to obtain analytic solutions for the piezomagnetic field due to the Mogi model (Fig. 1). It consists of inflated or deflated pressure spherical source within a semi-infinite magnetoelastic medium. The pressurized source with radius a, is buried at depth D, and the hydrostatic pressure change ΔP occurs within the sphere (Table 1). The elastic medium is supposed to be magnetized from the ground surface to the depth of the Curie point isotherm, except for the interior of the spherical source. The internal area of the source is regarded as being demagnetized due to the high temperature of magma.

The solution of integrals in eq. (3) for a piezomagnetic field due to an Okada model (Fig. 2) is given by Sasai's (1991b) formula, limited to the case of a vertical fault. Recently, Utsugi *et al.* (2000) extended

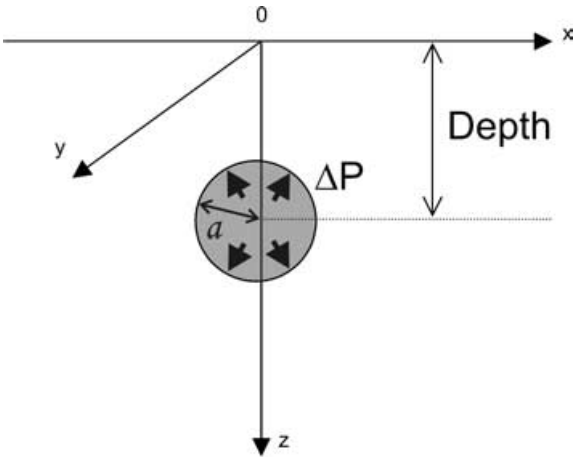

Figure 1. Mogi's source: a hydrostatically pumped pressure source in a homogeneous and isotropic elastic half-space with a uniformly magnetized upper layer centred at (0, 0, *D*) with radius *a*. The Curie point isotherm is at a depth *H*.

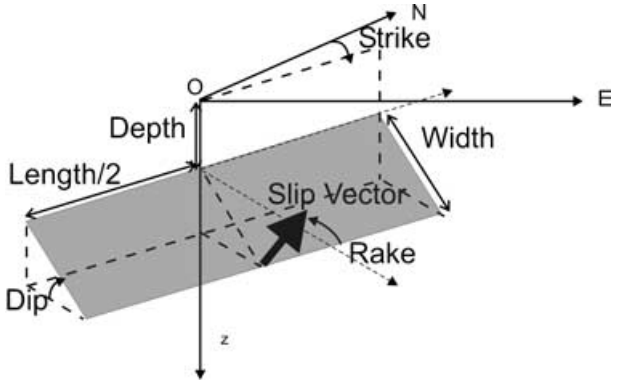

Figure 2. The Okada source: a fault occurring in homogeneous and isotropic elastic half-space with a uniformly magnetized upper layer. *H* is the depth of the Curie point isotherm. Depth is the distance between the origin *O* and the upper edge of the fault; Strike is the orientation of the fault with respect to the North; Dip is angle of the fault plane with respect the horizontal plane; Rake is the angle of the displacement; Length and Width are the length and width of the fault respectively; Slip is the module of the displacement.

Sasai's analytic solution to cases of an inclined fault including dip-slip. The parameters involved in the forward modelling for the Okada source are shown in Table 2.

2.2 Electrokinetic effects

Magnetic fields can arise from fluid flow circulating beneath the Earth's crust in the presence of an electric double layer at the solid–liquid interface (Fenoglio *et al.*1995). This double layer consists of immobile ions at the surface, usually negative for silicate minerals, and ionic charges distributed in the liquid phases according to the Boltzmann distribution (Nourbehecht 1963; Ishido & Mizutani 1981). It is a diffusive layer with an excess of positive ions with respect to negative ions in the proximity of the interface. Mathematically, the source is equivalent to a surface distribution of electric dipoles along the interface. This charge separation sets up an electric potential, known as streaming potential, generated by pore-

Table 1. Mogi Model sources parameters. The fourth column give the range value within which the synthetic models are generated.

Mogi model geometrical parameters	Symbol	Unit of measurement	Ranges
Volume of the spherical source	V	m^3	10^6–10^8
Depth of the centre of the sphere from the surface	D	m	200–3000
Sphere centre coordinates	[Xc, Yc]	m	−4000–4000

Table 2. Okada model parameters.

Okada model geometrical parameters	Symbol	Unit of measurement	Ranges
Dip fault	δ	degrees	0–90
Azimuth (° from North)	α	degrees	0–180
Depth	D	m	200–3000
Fault width	W	m	200–3000
Fault length	L	m	500–6000
Dislocation	u	m	1–3
Fault centre coordinates	[Xc, Yc]	m	−4000–4000

pressure gradients. The fluid flow produces an electric potential by means of electrokinetic phenomena and the resulting current flow will produce a magnetic field (Fitterman 1978, 1981).

The equations relating the electric current density j to the fluid flow density v are:

$$j = -\phi\rho\nabla E - \frac{\phi\varepsilon\zeta}{\eta}\nabla P, \tag{4a}$$

$$v = \frac{\phi\varepsilon\zeta}{\eta}\nabla E - \frac{k}{\eta}\nabla P, \tag{4b}$$

where E is the streaming potential, P is the fluid pressure, ϕ is the porosity of medium, ε is the dielectric constant, ζ is the zeta potential, η is the viscosity of fluid and ρ is the electrical conductivity.

In the case of a homogeneous medium, the current density is:

$$j = -\phi\rho\left[\nabla E - \frac{\varepsilon\zeta}{\eta\rho}\nabla P\right] = -\phi\rho\left[\nabla E + C\nabla P\right], \tag{5}$$

where the C coefficient is the streaming potential coefficient. At any time t, the electrokinetic magnetic field (B_{ve}) observed at the ground surface is given by:

$$B_{VE}(Q,t) = \frac{\mu_0}{4\pi}\nabla\times\iiint_{V_E}\frac{j(M,t)}{r}\,dV_M, \tag{6}$$

with Q the observation point and *j(M, t)* the electrokinetic current at the time t and in a point M of the volume V_E affected by the fluid flow.

A series of studies elaborated by Fitterman (1978, 1979, 1981) demonstrated analytic and semi-analytic solutions for the electric and magnetic fields due to electrokinetic sources in horizontally layered and vertically faulted half-space, while Ishido & Mizutani (1981) provided fundamental data of the parameters for the electrokinetic coupling through laboratory experiments. Fitterman (1978) computed the electrokinetic magnetic field at the ground surface for a spherical pressure source in a layered earth. He proved that the magnetic field due to the current flow is identically zero on the ground surface, independently of the number of layers and the pressure sources (Fitterman 1978). Using Edward's (1974) approximation, Murakami (1989) extended Fitterman's solutions to the case of inclined fault separating two media with different streaming potential, $C1$ and $C2$. The electrokinetic source intensity

Table 3. The magnetic properties are fixed to values that resembles cases likely to occur in volcanic areas.

Magnetic parameters	Symbol	Unit of measurement	Value
Average magnetization	J	A m^{-1}	5
Curie depth	H	m	15 000
Magnetic inclination	I	Degree	53
Magnetic declination	D	Degree	1
Piezomagnetic model parameter			
Rigidity	μ	bar	3×10^5
Poisson's ratio	ν	0.25 ($\lambda = \mu$)	0.25
Stress sensitivity	β	bar^{-1}	0.0001
Electrokinetic model parameter			
Streaming potential of upper side	C1	mV/bar	20
Streaming potential of lower side	C2	mV/bar	10
Electric conductivity of upper side	ρ_1	S/m	0.01
Electric conductivity of lower side	ρ_2	S/m	0.1
Source function	S	Volt	1

$S = (C1 - C2)P$ is constant and bounded by the fault geometry. No source exists outside of this region. The corresponding magnetic parameters are listed in Table 3.

2.3 Thermomagnetic phenomena

The thermo magnetic effect may play an undoubted role on active volcanoes, where large amounts of thermal energy concentrate and dissipate in short time lapses through fumarole activity and emission of lava and ash. Rocks subjected to temperature change are also submitted to demagnetization and/or remagnetization. When the temperature exceeds the Curie point, the rocks lose their magnetization and consequently modify the static crustal magnetic field (Rikitake 1952; Rikitake & Yokoyama 1955). Conversely, emplaced lava flows or pyroclastic deposits that cool below their Curie temperature, acquire a thermo-remanent magnetization that is related to intensity and direction of the Earth's magnetic field (e.g. Stacey & Banerjee 1974).

If a sphere is uniformly demagnetized, the anomalous field due to the demagnetization process is equivalent to a dipole situated at the centre of the sphere having an orientation anti-parallel to the direction of the original magnetization. The change in the total intensity (ΔF) at position (x, y, 0) caused by a spherical source located at (0, 0, z) is given by:

$$\Delta F = -\frac{M}{4\pi r^3}\left\{1 - 3\left(\frac{x}{r}\cos I - \frac{z}{r}\sin I\right)^2\right\}, \tag{7}$$

where M is the intensity of the magnetic moment of the source, r is the distance between the centre and the observation point, x the horizontal projection of r and I the inclination of the ambient geomagnetic field (Hamano *et al.* 1990).

Magnetic anomalies due to thermal demagnetization with arbitrary shape can be calculated by integrating dipole sources. We can also utilize some semi-analytic solutions to reduce the dimension of volume integral such as those proposed by Talwani (1965). The magnetic anomaly field produced by a non-magnetized prismatic body was firstly derived by Bhattacharyya (1964). The model parameters and the medium constants are summarized in Table 4.

Table 4. Parameters for prismatic body.

Prismatic body geometrical parameters	Symbol	Unit of measurement	Ranges
Depth	D	m	200–3000
Width	W	m	200–3000
Length	L	m	200–6000
Thick	T	m	200–1000
Fault centre coordinates	[Xc, Yc]	m	−4000–4000

3 THE INVERSION TECHNIQUE

Volcanomagnetic inverse problems involve the analysis of appropriate numerical strategy to identify the source parameters of a wide spectrum of volcanomagnetic anomalies recorded on active volcanic areas. As the magnetic models are highly non-linear and characterized by a high number of parameters, the inverse numerical problem could be difficult to solve by applying methods based on linearization of the problem. On the other hand, a trial and error procedure for solving the magnetic inversion problem may take long time and the quality of the results might not be enough accurate. Artificial neural networks (ANN) have been proposed to overcome these drawbacks. Techniques based on ANN allow implementing inversion schemes characterized by good robustness and high computational speed, once the neural network has been trained to solve the inversion problem. However, the neural approach proved less accurate than the GAs optimization algorithm for both Mogi and Okada models (Del Negro & Nunnari 2003). Indeed, all the methods based on ANN inversion approach start from the assumption that the function to be inverted exists and is both continuous and smooth. Because of the complexity and the non-linear structure of the equations of volcanomagnetic models, it is not possible to mathematically proof these hypotheses. Furthermore, non-linear models, such as magnetic models, can be extremely difficult to optimize due to the presence of inherent discontinuities or local optima, where techniques based on the gradient methods are likely to get stuck. Since the parameter space is typically very large, multimodal, and poorly understood, GAs have the advantage of imposing constraints on parameter space to ensure that results are meaningful and feasible. Hence, GAs perform a much broader search over the model space, with a greater likelihood of finding the global optimal solution (Holland 1975).

Roughly speaking, the adopted GA search algorithm randomly generates a set of initial parameters, whose values are constrained within a prefixed range. Using the analytical model, a population of magnetic anomaly fields is computed for this set of parameters. The solutions are tested by an objective function that quantifies the degree of correlation between model and observed data from the field. The solutions are ranked, from the best to the worst, according to the objective function and new set of likely solutions are generated from the best solutions by the laws of evolutionary genetic. The evolutionary algorithm uses a collection of heuristic rules to modify the population of trial solutions in a way that the next generation tends to be on average better than its predecessor. Heuristic selection and replacement operators (uniform–random selection or roulette selection) are then used to sample the best solution in the current population for reproduction at each generation (Goldberg 1989). Well-known genetic operators, crossover and mutation, make the population evolve from one generation to the next (Michalewicz 1992). This procedure is repeated for a large number of generations until the best solution is reached. Because of the initial random and progressively more deterministic evolution of the parameter space, GA algorithm offers the possibility of efficiently and rapidly locating the most promising solution. From its initial random distribution in the parameter space, the population progressively converges

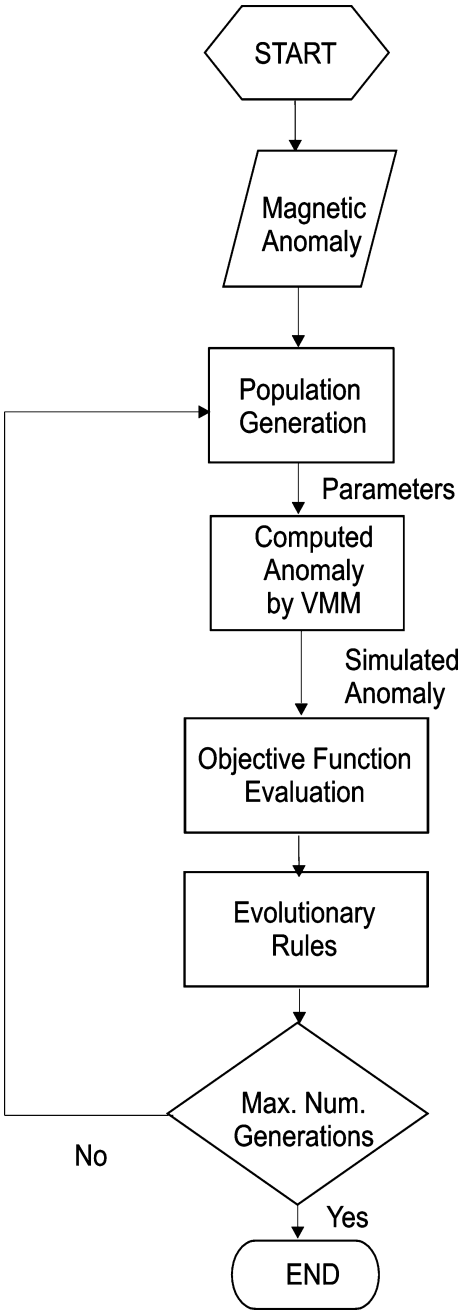

Figure 3. Schematic of GA inversion.

to the solution that minimizes the objective function. A simplified schematic diagram of the procedure is shown in Fig. 3.

The objective function that quantifies the difference between the observed magnetic data and the model computed for each potential solution is evaluated using the value of the reduced chi-square that accounts for the measurements error defined by the standard deviation σ, as:

$$\chi^2 = \frac{1}{d}\sum_{i=1}^{N}\frac{(O_i - M_i)^2}{\sigma_i^2}, \tag{8}$$

where $d = N - P$ is the degree of freedom, N represents the number of measuring points, P is the number of parameters, while O_i and M_i indicate the observed and modeled magnetic field values at each point, respectively.

The inversion scheme (Fig. 3) was considered in order to assess the accuracy of GA to estimate the optimum source parameters for magnetic models from observed magnetic data. The main reason for studying the accuracy of the inverse solution is that the volcanomagnetic inverse problem depends on several aspects such as the number of recording stations, their geographical distribution on the ground, the position of the source with respect to the recording network and so on. Since it is not possible to answer these problems from a theoretical point of view due to the high non-linearity of the problem and the huge number of elements that could play a role in the existence and uniqueness of an optimum solution, we have investigated the reliability of modelling procedure on synthetic data generated using the VMM forward modelling program that gathers the theoretical magnetic models referred in the previous section.

4 TEST ON SYNTHETICALLY GENERATED ANOMALIES

We carried out several inversion tests on synthetic data set generated by using the Mogi and Okada forward models. The error estimation for a magnetic inversion is complicated by the non-linear nature of the search parameter space. Moreover, the presence of noise in the data affects the accuracy of the estimates, preventing the algorithm from locating the true solution in the parameter space. The effect of the noise on the accuracy of the GA solution is more than proportional as a consequence of the non-linearity of the model equations (Ramillien 2001). The robustness of GA inversion algorithm was investigated on data corrupted by random Gaussian noise (Nunnari *et al.* 2001; Del Negro & Nunnari 2003) and the procedure was found to be robust enough.

Indeed, the accuracy of the solution is also dependent on both the number of available stations and their distribution with respect to the geophysical source position. Since the continuously operating magnetic stations on a volcano are usually very limited, we have examined the accuracy of the inversion procedure as the spatial density of stations decreases. For this test the data set was supposed to be noise free. The experimental framework was formulated as follows. As a general study case, we assumed a uniform distribution of magnetic observation points (stations) within a regular grid of 10 km $\times$ 10 km, hypothesized to be centred on the summit of volcanic area. To statistically evaluate the accuracy of inversion, 100 models with uniformly distributed parameters, whose values were fixed in ranges that resemble likely cases in volcanic area, were inverted. The goodness of the inverse modelling approach was calculated by an appropriate performance index:

$$\text{NMAE}\,\% = \frac{100}{(N \cdot \text{Range})}\sum_{i=1}^{N}|P_{Ci} - P_{Ti}|, \tag{9}$$

where N is the number of considered models, P_{Ti} is the generic ith parameter of the calculated model, and P_{Ci} is the corresponding true parameter.

The magnetic parameters (e.g. the average magnetization, the magnetic declination, etc.), implied in the models, can be estimated from geological properties of the volcanic areas, thus it is unnecessary to overload the inversion algorithms by including them as further parameters to be estimated. The values of the parameters of the magneto-elastic medium used in these calculations are shown in Table 3. The models are embedded in an elastic homogeneous Poissonian half-space (Poisson's ratio = 0.25, i.e. Lame's constant $\lambda = \mu$), a reasonable approximation in volcanic areas (i.e. Sasai 1991b; Russo *et al.* 1997).

4.1 Results using the Mogi type model

Since the piezomagnetic effect for a spherical source linearly depends on the product $a^3\Delta P$ (Sasai 1991a), it does not make sense to invert a and ΔP individually because the inverse problem becomes undetermined. Hence, in the Mogi model, the influences of changes in pressure and in the radius of the sphere on the amplitude of the magnetic variation cannot be separated, that is, observed magnetic changes can be produced by a small sphere with a large pressure change or a large sphere with a smaller pressure change. Consequently, radius and pressure retrieved by the inversion may be physically unrealistic. For a spherical source, the change in radius, Δa, of a source with radius a, caused by a pressure variation ΔP is given by Hagiwara (1977) as

$$\Delta a = \frac{a\Delta P}{4\mu}, \tag{10}$$

where μ is the Lame's constant. As long as a is large with respect to Δa, the volume change ΔV of the spherical source may be estimated as the surface area of the sphere ($4\pi a^2$) times the change in radius:

$$\Delta V = \frac{\pi a^3 \Delta P}{\mu}. \tag{11}$$

Considering the above equation, it can be seen that the volume variation is the noteworthy parameter. Substituting the expression (11) in the Sasai's solution (1991a), the values of pressure change and the radius can be disregarded, and only the change in volume ΔV needs to be inverted (Table 1). For piezomagnetic anomalies, the NMAE% performance indices on all the models inverted is computed varying the number of measurement points within the regular grid (Fig. 4). It can be noted that the inversion modelling has no problems attributable to ambiguity of the solution when the number of observations is appropriate (say 4 × 4 or larger); in such a case the NMAE%, is very low for all the model parameters (less than 1 per cent). On the contrary, when the number of measuring points is restricted (say 2 × 2) the NMAE% tends to suddenly increase; this indicates that the search problem is no longer well constrained. It should be noted that in this latter case the number of measurement points is equal to the number of searched parameters, which in a linear context is the minimum number of measurements needed to obtain a non-ambiguous solution. Analogous results were obtained (Fig. 5) when the thermomagnetic effect is considered. Also in this case all the model parameters were estimated with high accuracy, while the error tends to suddenly increase with a number of stations less or equal to 2 × 2.

4.2 Results using the Okada type model

Similar tests were performed for the Okada piezomagnetic model, which involves a higher number of parameters (10) and is characterized by more complex non-linear analytical expressions (Sasai 1991a; Utsugi *et al.* 2000). Particularly, we report the results obtained for a strike-slip fault source. To assure the convergence versus the optimum solution, initial tests were carried out to determine the best GA settings (e.g. initial population, number of generations, crossover probability, etc.). As expected for such a complex non-linear model, the initial population should have been increased up to 500 individuals and a larger number of generations were required to enhance the accuracy. Similarly to the experimental framework assumed for the Mogi source, we inverted 100 models, whose parameters are allowed to vary in an interval widely representative of possible real situations (Table 2). Results obtained are shown in Fig. 6. Compared with the Mogi case here it is possible to see

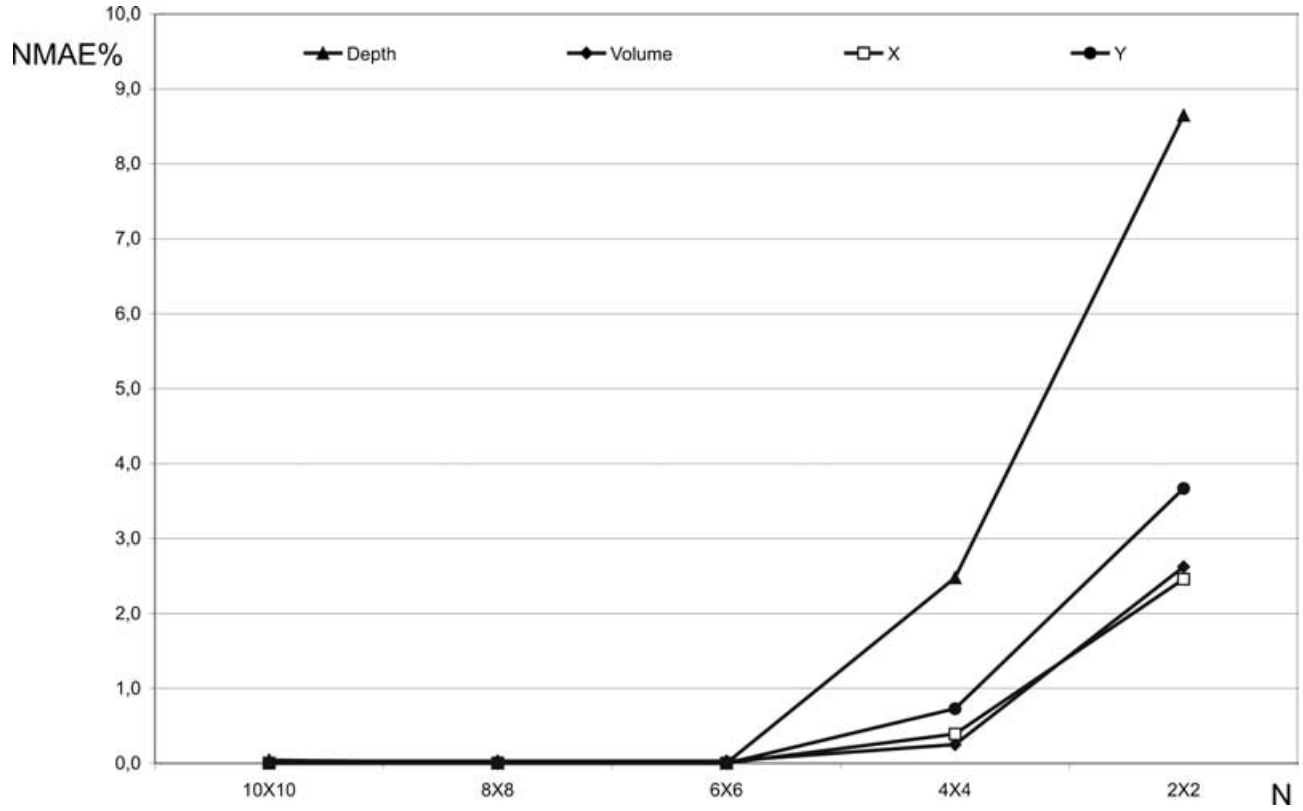

Figure 4. The NMAE% performance indices for the piezomagnetic Mogi model as the number of measuring points decreases.

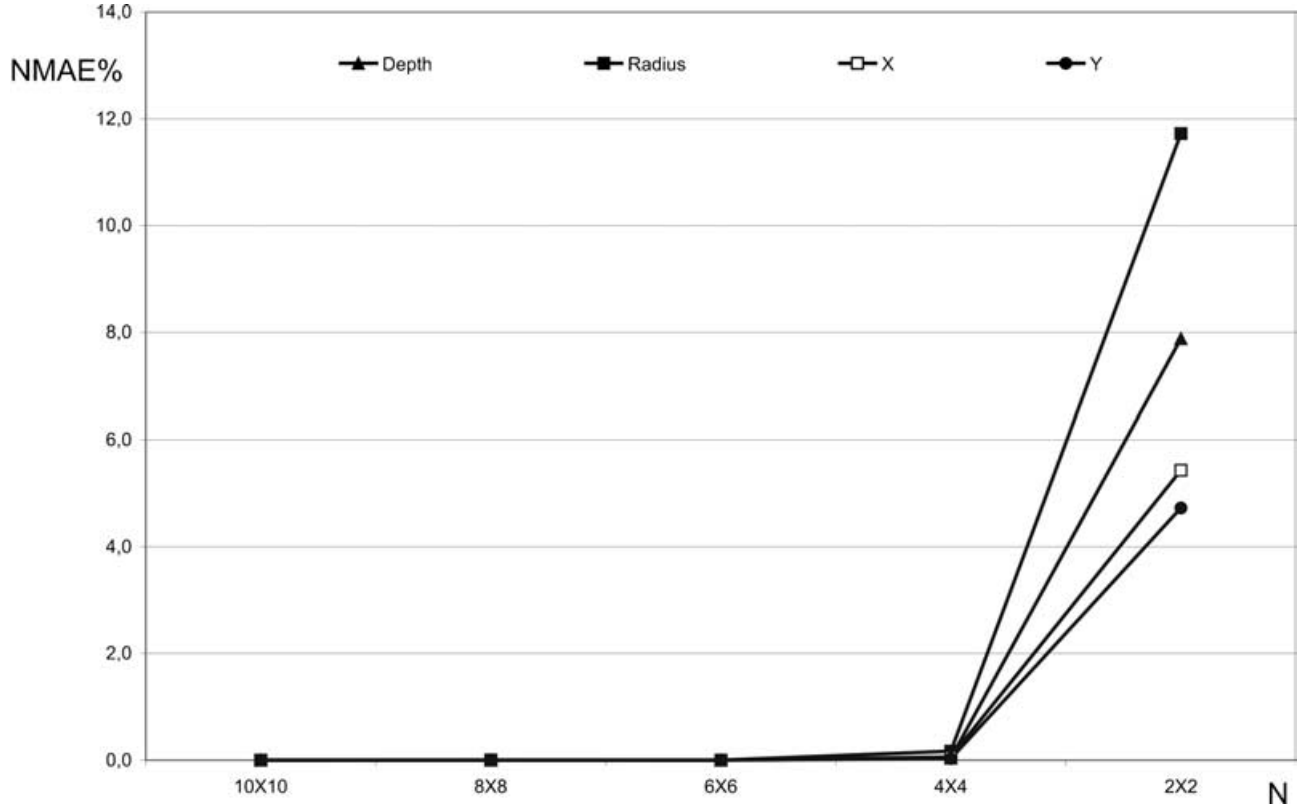

Figure 5. Performance indices computed over 100 thermomagnetic Mogi models.

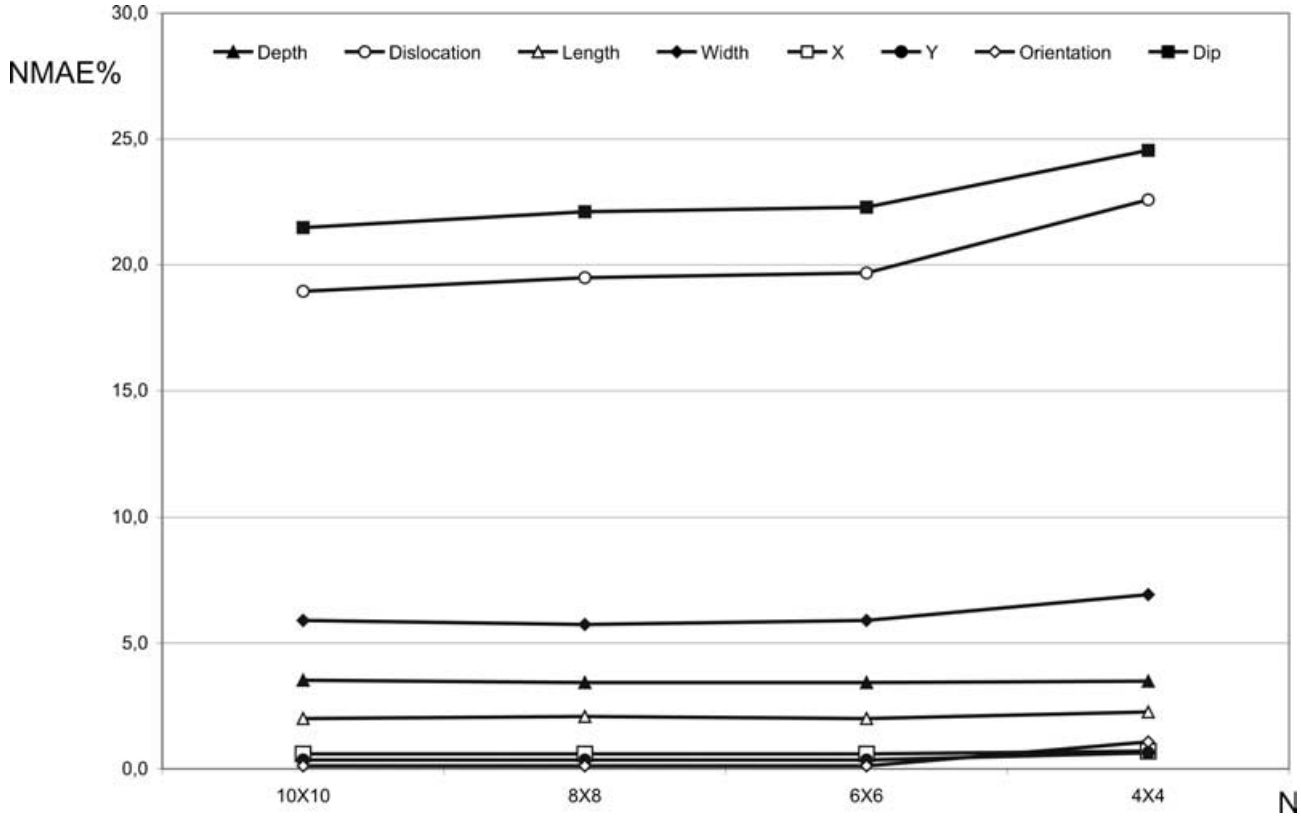

Figure 6. The NMAE% performance indices for the piezomagnetic Okada model.

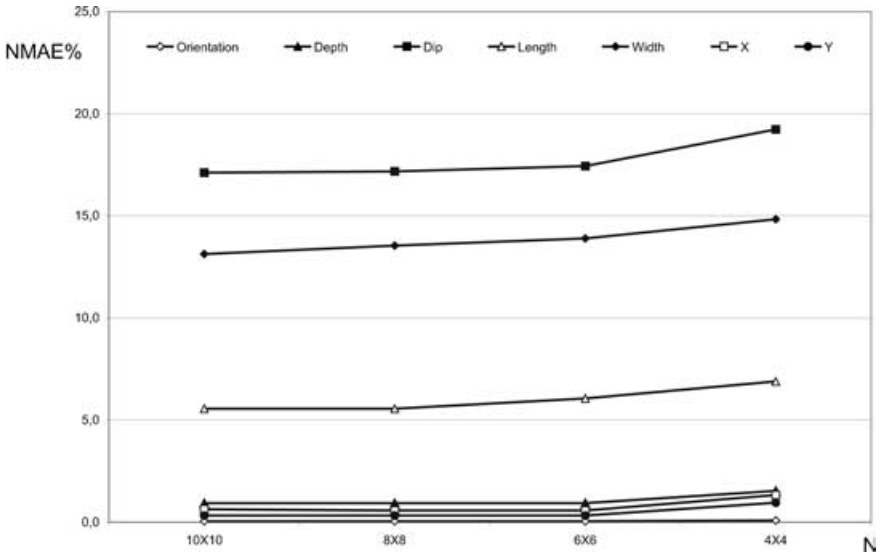

Figure 7. Performance indices obtained in the case of electrokinetic Okada models.

that estimation is less accurate even with a 10 × 10 regular grid is assumed. Indeed the eight parameters can be classified into two subsets: the first set including the parameters X, Y and orientation, which estimated with a NMAE% less than 1 per cent with a regular measuring array 4 × 4; the second set, which includes the parameters depth, length, width, dip and dislocation exhibits a NMAE% ranging between 2 and 25 per cent even in the best case (10 × 10). Further investigations with a larger array (50 × 50) confirm that the NMAE% for the second subset remains larger respect to the first subset, even if it decreases.

Similar results were achieved for the Okada electrokinetic model that involves seven parameters to be inverted (Table 2). Since the ρ and S magnetic parameters are linearly related to the magnetic field anomaly, as can be seen from the analytical solution (Murakami 1989), they were not taken into account in the inversion procedure. Once the inversion problem is solved, this linear relationship allows for estimating the ρ and S parameters starting from the magnetic field data and the inverted solution. It was assumed that $S = 1$ V, in accordance with Murakami (1989), as this value is consistent with conditions expected in volcanic areas. Also in this case it is possible to recognize two subsets parameters: the first includes Orientation, X, Y, depth; the second gathers the width, length, dip (Fig. 7). Again, the first subset includes parameters characterized by a high level of accuracy (NMAE% less than 2 per cent) while the second subset exhibits an NMAE% ranging between 5 and 20 per cent. These results agree with Nunnari *et al.* (2001) who reported that areal parameters (width and length) and dip are difficult to invert also by using a different inversion technique based on ANN.

4.3 Results using the rectangular prism type model

The thermomagnetic effect due to rectangular prisms was implemented considering analytical expression provided by Bhattacharyya (1964). The experimental framework is the same as above. In Table 4, the geometric and location parameters of this type of source are reported together with the associated ranges, while the NMAE% obtained is shown in Fig. 8. The dykes are assumed to have an elongated shape. It can be seen that the source position (depth and centre coordinates of the prism-shaped body) is retrieved with high accuracy (less than 1 per cent) even with 4 × 4 measuring points. The length parameter is estimated with accuracy better than 2 per cent for a 4 × 4 observation array, while the remaining parameters (width, thickness) exhibit a larger NMAE% ranging between 20 and 35 per cent.

4.4 General considerations

As a general result, we have found that source location parameters are retrieved with high accuracy in all the considered models and for all the type of studied physical mechanism. The lower accuracy observed for the other parameters could be attributed to a difficulty of GA to converge in a fixed number of generations toward the global minima because of a low sensitivity of the objective function with respect to some parameters. Regarding the Okada electrokinetic model, sensitivity tests to each parameter were performed on a single source located at the centre of the grid at depth of 400 m. The value of other parameters were: orientation angle 30°, dip angle 45°, length 2000 m and width 1000 m. In each case, we varied one parameter at a time, while the others were kept constant.

In Fig. 9 the residuals in nT are plotted versus the considered variable. Analysis on the sensitivity functions confirms our hypothesis. Although the Xc and Yc sensitivity functions show two local minima, they are located at such a high residual that, the GA is able to escape from them. This is the reason why the location of the source is determined with high accuracy. Analogously, the sensitivity with respect to the orientation angle is a steeply varying function. The least sensitive parameter is the dip angle whose sensitivity function shows an asymmetric minimum (Fig. 9). It can account for the lower accuracy found out by the GA inversion for this parameter. We have tried to invert the seven parameters associated with this source and statistically compute the error over 20 inversions. In each of the 20 runs of the GA, the algorithm converges to the close neighbourhood of the true solution, starting with different random initial populations. The mean value and the standard deviation computed over the 20 results of the inversions are reported in Table 5. In agreement with the previous results, the parameters of the second subset are spread out around the mean value. Further tests were performed to better understand the behaviour of dip and width parameters. We have repeated the synthetic test on 20 different models over a 4 × 4 point grid and we have searched only for these parameters while the

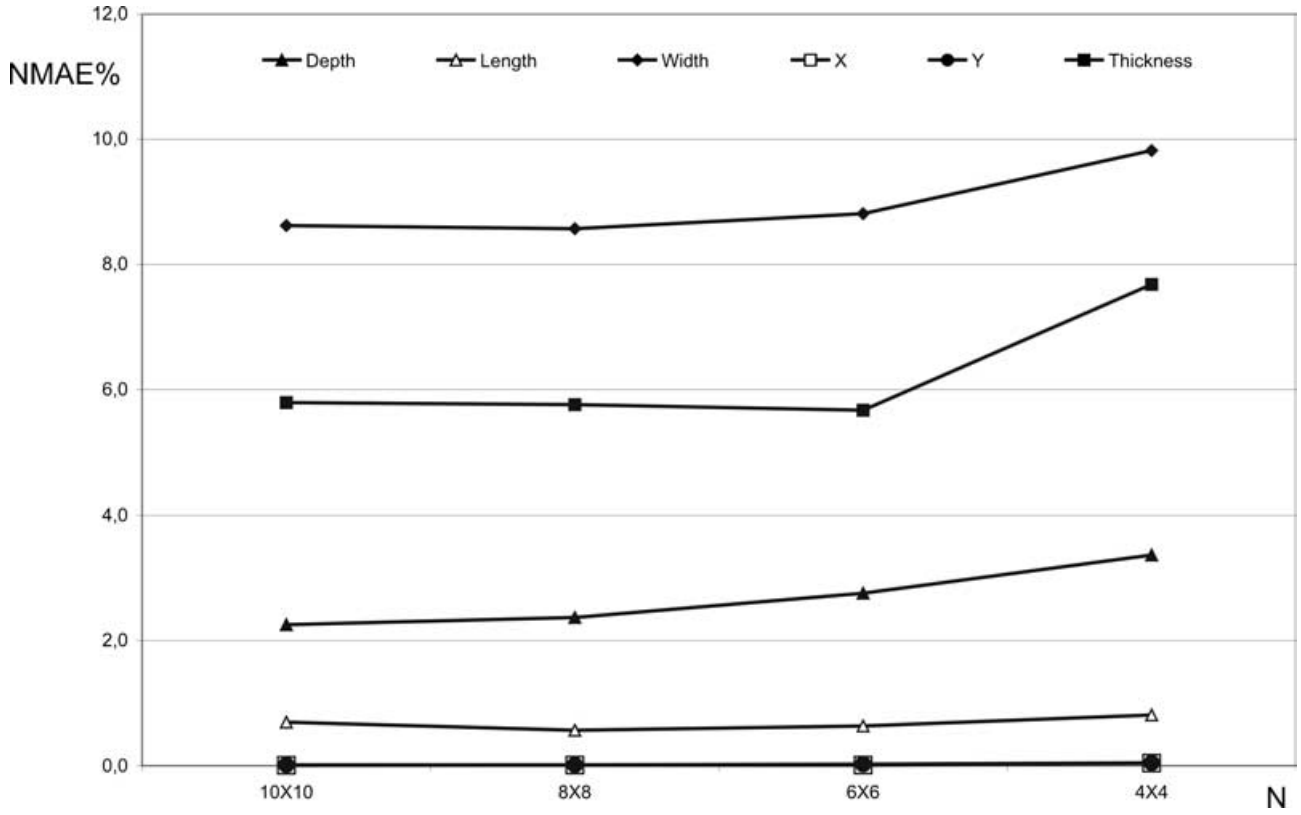

Figure 8. The NMAE% performance indices for the prismatic type model.

others were taken constant to the known values. In few generations the parameters are identified with a standard deviation of 28 m for width and of 0.2° for the dip angle, as shown in Fig. 10. Here, the known values versus estimated values are shown when two (Figs 10a and b) and seven (Figs 10d and e) parameters are simultaneously searched. It is evident that points in the second case are spread-out on a larger area with respect to the first. When only two parameters are searched, points are perfectly aligned along the bisector showing that the algorithm is capable of finding the true value with high accuracy. These results further confirm that the rather low accuracy for the width and dip parameters, when they are searched all together with the others, could be attributed to the difficulty of GA algorithm to converge towards the minimum in these circumstances. We also compared the errors on dip and width parameters both when two (Fig. 10c) and seven (Fig. 10f) parameters are simultaneously searched. It should be noted in the latter case that the nature of the model itself causes the GA to locate fault with larger width for a lower dip, but to more often find smaller width for higher dip. This feature could have implications not only for this inversion technique, but for others performed using electrokinetic fault models. To overcome these drawbacks, the number of initial individuals of the GA could be increased to enhance the number of possibilities to explore the overall parameter space (Goldberg 1989). In particular, if the population is too small (e.g. less than 100), the algorithm can converge too quickly to a local minimum of the objective function, but if it is too large the time of computation increases drastically. Since the parameters of the first subset are found with high accuracy in a few steps of generations, they can be suddenly retrieved and the search can be restricted only to the second subset. Hence, we propose a two-step searching procedure: firstly, we search for the parameters having high accuracy; secondly, we search for the second subset of parameters. This provides a reliable suboptimal solution with a good compromise between the efficiency and the computation time. An important decision in terms of efficiency of the two-step optimization techniques is when to stop the first step and begin the subspace search. Two possibilities are available: (1) waiting for no improvements in the objective function for few generations or (2) waiting to fall below a predetermined threshold. Research to define effective criteria suitable for choosing the stop criteria of the inversion is ongoing.

5 CASE STUDIES

To appreciate the strength of the proposed inversion scheme in real contexts, we report two case studies performed on field data. The first case refers to the inversion of an intrusive episode occurred during the 1989 Mt Etna eruption, involving the thermomagnetic effect. The second case study relates to magnetic anomalies recorded on Miyakejima volcano that was interpreted in terms of piezomagnetic effect.

5.1 1989 Mt Etna eruption: thermomagnetic anomalies of a shallow dyke

During the 1989 eruption of Mt Etna, two fracture systems opened at the foot of its 3000-m-high southeast crater and, trending *ca.* N45°E and N150°E, propagated quickly downslope to a distance of *ca.* 3 and 7 km, respectively (Fig. 11). The northeastern fracture fed a flank eruption, whereas the south-eastern remained dry and offered contrasting volcanological and geophysical evidence of the presence of magma at a shallow depth. During the opening of this non-eruptive fracture system, a differential magnetic network was set up on a short

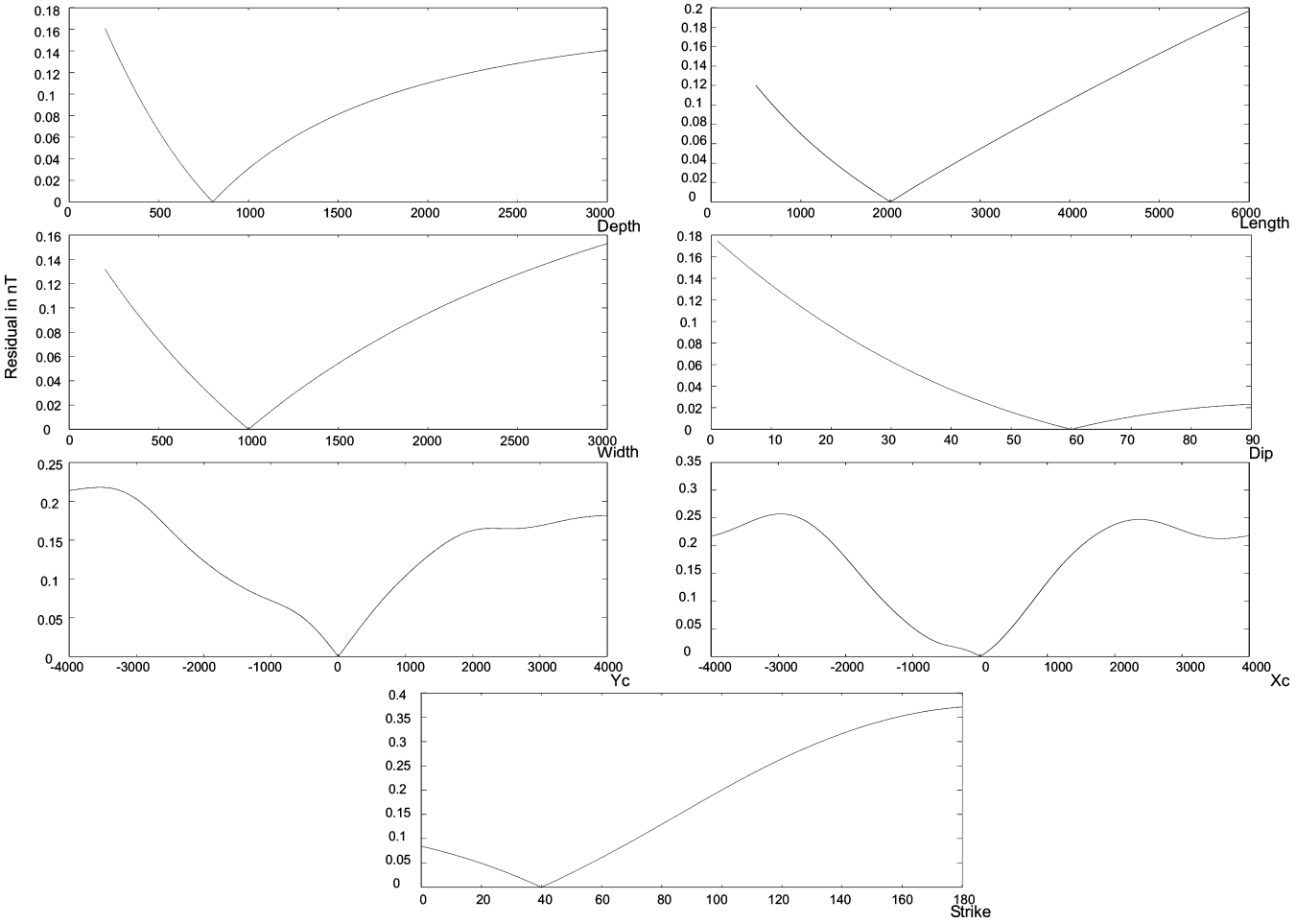

Figure 9. Sensitivity of fit to electrokinetic Okada source parameters.

Table 5. Parameters of the electrokinetic Okada source. The mean value and the standard deviation are computed over the estimated parameters obtained by 20 different runs of GA.

Parameter	Value	Mean value	Standard deviation
Dip	60°	50.35°	15.65°
Strike	40°	39.83°	0.36°
Length	2000 m	2004.33 m	64.43 m
Width	1000 m	1262.46 m	377.53 m
Depth	800 m	789.82 m	22.38 m
xc	0°	54.73 m	67.11 m
yc	0°	−12.47 m	20.16 m

profile across its distant extremity. Initially, the magnetic field did not display any change along the profile between frequent surveys. However, repeated measurements at intervals of about 3 months for 2 years revealed the slow buildup of a 130 nT anomaly. The anomaly vanishes laterally within 0.2 km from the surface expression of the fracture system. The strong spatial stability in time of the anomaly, its total amplitude and the duration of the anomaly-growth phase, all suggest its thermal origin. In particular, it is likely that a newly injected magma body at shallow depth produced the local magnetic changes observed. This exceptional set of observations constrains the location and time of cooling of a shallow dyke.

A slowly cooling dyke, indeed, acquires a thermo-remanent magnetization which is related to the intensity and direction of the Earth's magnetic field and to the mineralogy of the dyke (e.g. in Stacey & Banerjee 1974). The local static magnetic field is slowly modified by the changing magnetization of the embedding rocks and the dyke (e.g. in Rikitake 1952). The duration of such changes may range from weeks to years, and magnetic anomaly amplitudes in the order of several tens of nanoteslas have been reported (e.g. Zlotnicki & Bof 1998). Formulation of a time-varying thermomagnetic model of a freezing dyke is very complex since it needs opportune hypothesis on the thermomagnetic properties of rocks and a suitable thermal model of the dyke itself. Del Negro & Ferrucci (1998) used a magnetization of 8 A m^{-1} (the mean natural remanent magnetization for 1910 and 1950 lava flow samples) for the country rock at ambient temperature, and gave a 50 per cent magnetization (i.e. 4 A m^{-1}) to the dyke in September 1991. Between the dyke and the country rocks it was also supposed a small thermally anomalous band, limited in thickness by the low thermal diffusivity values of lavas, where temperatures rapidly grow inwards: overall, and from a magnetic standpoint, this means that the effective dyke cross-section is enlarged. The magnetization of this layer varies with temperature from the dyke walls to the country rocks kept at ambient temperature.

According with the thermomagnetic model by Del Negro & Ferrucci (1998), the GA was requested to search the best solution for the parameters of the intruding dyke and the anomalous band whose range values are reported in Table 6. The set of likely models could be significantly restricted by the location of the ground surface

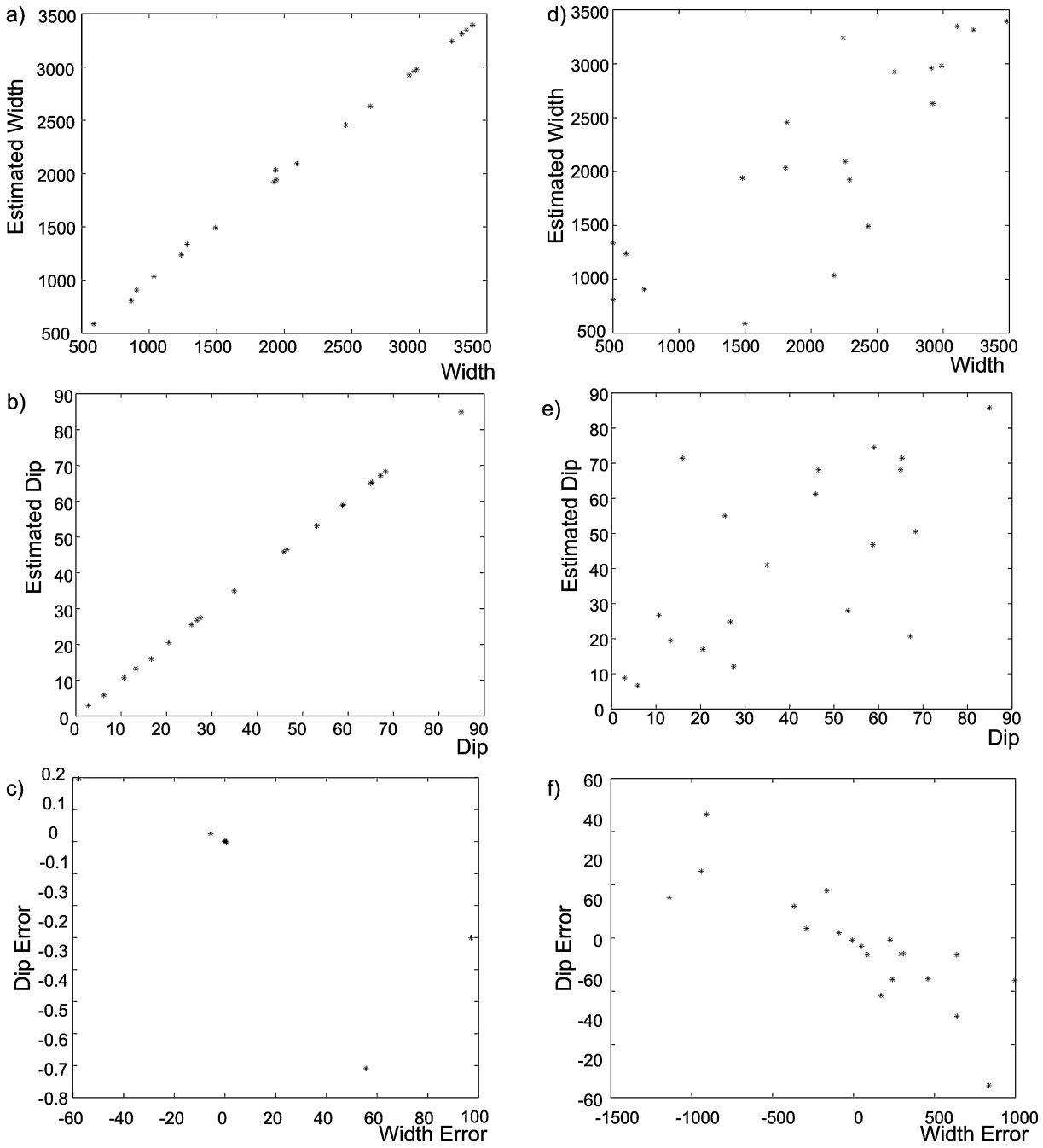

Figure 10. True versus estimated Width and Dip parameters when the parameters simultaneously searched are two (a, b) and seven (d, e). The errors on Dip and Width parameters are also compared for the two cases (c, f).

fractures and by the availability of geophysical evidences yielded by the small spatial extent of the anomaly. The data set used for the inversion consists of 447 total magnetic field measurements carried out on September 1991 along the profile at a spatial interval of 5 m. The GA inversion converges versus a best solution (Table 6) with a reduced chi-squared (the objective function) of 1.5 (Fig. 12). The robustness on each parameter of the solution was taken into account in the analysis to assess the goodness of the proposed model. The best solution can be accepted as the global minimum, when it can be reproduced over several runs as a stable solution. To appraise the robustness of the obtained solution we performed a number of GA inversions. The initial population was initialized with a number of different random values, and the GA always converged to the neighbourhood of the same solution, proving its relative robustness. Our model fits the data well enough to assess that the anomaly observed is compatible with that of a intrusive dyke.

5.2 Magnetic anomalies during the 2000 Miyakejima volcano eruption

Remarkable volcanomagnetic changes have been reported in association with the renewal of the eruptive activity in volcanic areas (Zlotnicki & Bof 1998; Del Negro & Currenti 2003), however, very few volcanoes world wide are monitored by magnetic arrays with

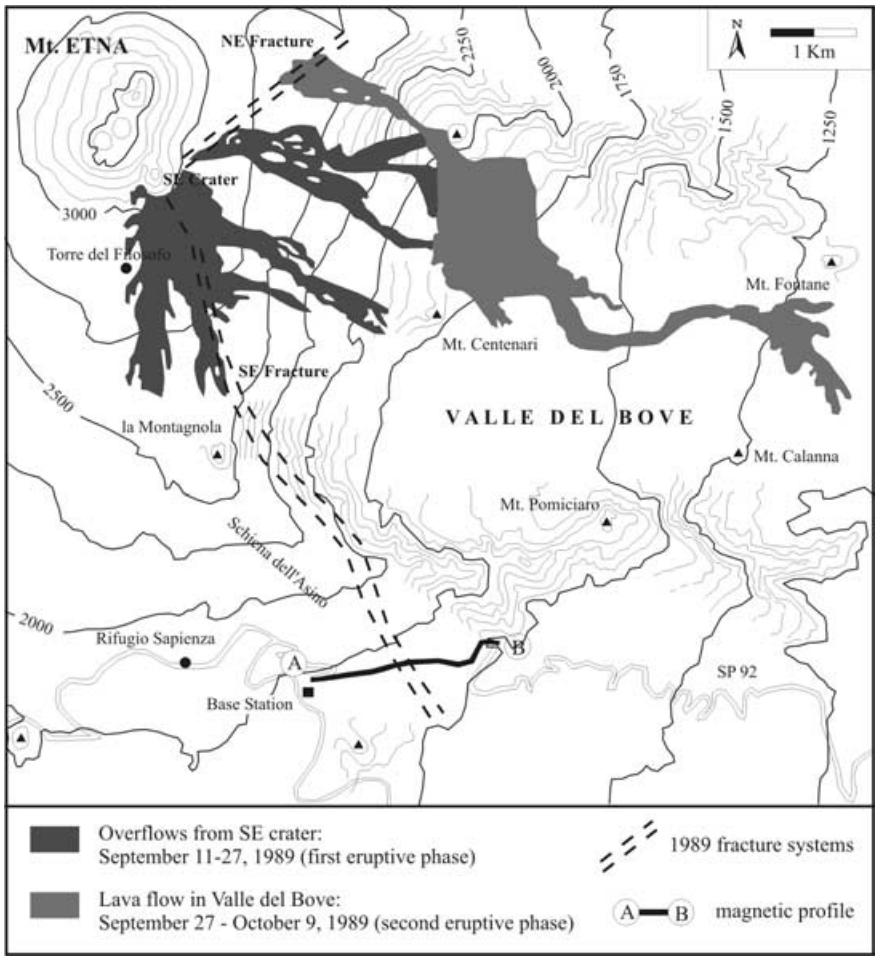

Figure 11. Location map of the fracture systems which opened and developed during the 1989 eruption of Mt Etna.

Table 6. Parameters for the intrusive dyke modelling the anomaly recorded during the 1989 Etna eruption.

Model parameters	Symbol	Unit of measurement	Ranges	Obtained parameters
Depth of dike	D_1	m	100–600	450
Width of dike	W_1	m	100–500	500
Thick of dike	T_1	m	1–10	4.5
Depth of anomalous band	D_2	m	20–100	34
Width of anomalous band	W_2	m	500–1000	900
Thick of anomalous band	T_2	m	20–100	10

enough stations to allow for reliable inversion. An exemplary case study was provided by the magnetic observations carried out during the 2000 eruption of the Miyakejima volcano, which is monitored by a high number of stations well distributed over the volcano edifice since 1995 (Sasai *et al.* 2002). High quality magnetic data were recorded simultaneously at several magnetic stations. Step-like variations in the total magnetic intensity were also accompanied by electric field variations recorded at the occurrence time of large tilt-step events. They indicate an up-ward motion of the summit area, which suggested a subsurface expansion under the central crater of the Miyakejima volcano (Ukawa *et al.* 2000). This indicates that the magnetic variations are maintained by the stress build up accompanying the tilt step. This is one of few examples of such observations in which magnetic fields vary simultaneously with a rapid mechanical event. The amplitude and the timescale of the magnetic changes pointed to the piezomagnetic effect as the main physical mechanism leading to these variations. The detected magnetic variations were consistent with the Mogi piezomagnetic model, which well explains the amplitude and the polarity of the magnetic changes detected simultaneously at more stations (Sasai *et al.* 2002). Starting from the assumption of a Mogi source model, the GA inversion procedure was applied to prove the capability to identify model parameters for the July 14 tilt-step event (Fig. 13). The set of all potential mathematical solutions were constrained into the range of possible variations according to geological evidences, which play a crucial role in identifying the piezomagnetic model (Tanaka *et al.* 1999). We set up an inversion scheme using the GA algorithm based on data recorded at five stations (Fig. 13). The solution given by the GA inversion scheme is a sphere located at 1 km southward from the central craters, at a depth of 3500 m, and with a volume change of 3×10^6 m^3. This solution is quite similar to that found by Sasai *et al.* (2002) using a trial and error procedure.

To strength the reliability of our solution, a sensitivity analysis was performed on the source parameters (Tiampo *et al.* 2004a). Only one parameter of Mogi model was varied at a time, while the remaining three were kept constant. The residual (in nT) was computed and plotted versus each parameter (Fig. 14). As can be seen, all the sensitivity functions exhibit a single global minimum, which proves the robustness of the searched solution (Tiampo *et al.* 2004b).

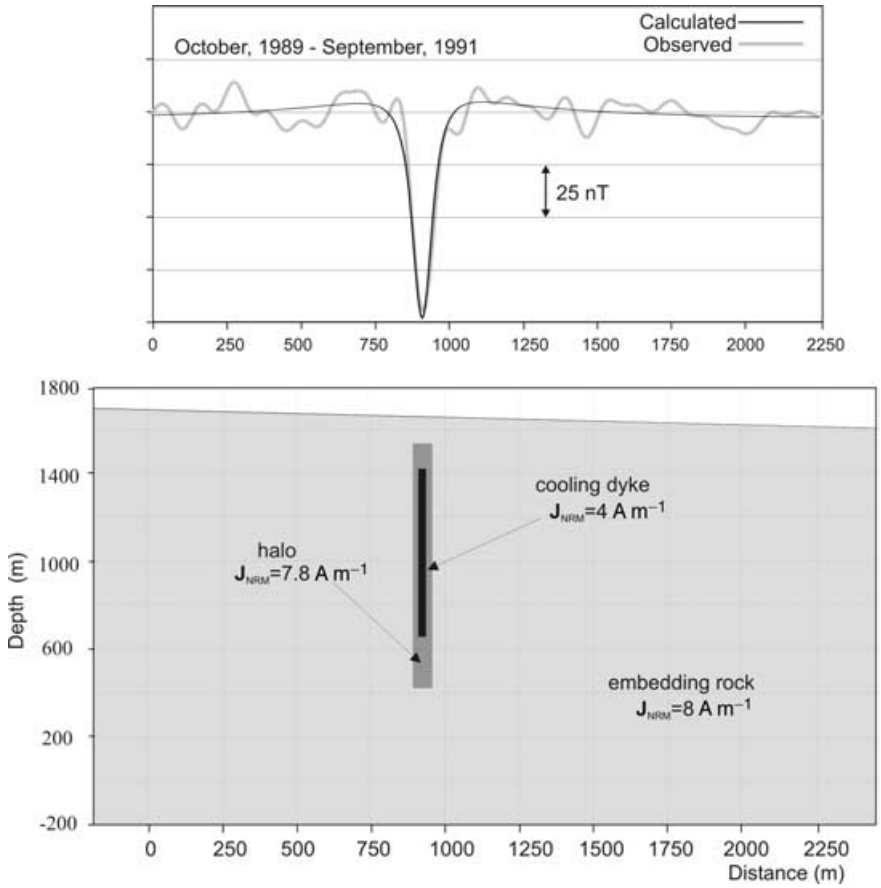

Figure 12. Thermomagnetic anomalies at Mt Etna: observed (grey line) and computed (black line).

6 CONCLUDING REMARKS

The inversion problem in volcanomagnetic modelling suffers from the ambiguity and instability of its solutions (Lavrentiev *et al.* 2003). The ambiguity arises from the inherent property of potential fields for which different combinations of parameters may lead to similar observations. Moreover, potential fields inversion is notoriously unstable. Because of ambiguity and instability of solutions, the volcanomagnetic inversion problem can be secured by narrowing the set of all possible solutions to a predefined solution class that allow for a unique and stable solution. The *a priori* definition of the geometry (simplified bodies: spherical, rectangular, prismatic) of searched anomalous body and the *a priori* recognition of the involved physical mechanism (thermomagnetic, piezomagnetic, electrokinetic effects) allows reducing the number of likely solutions considerably (Blakely 1995). Under these assumptions, an inversion procedure based on GAs was implemented for the estimation of the volcanomagnetic sources from the magnetic anomaly data. Lacking any analytical proof of the existence and uniqueness of the inverse solution, our experimental framework can be considered as an attempt to assess the goodness of the solutions for inverse modelling. The analysis allows answering questions about the uniqueness of the solution, the number of measuring stations, and the accuracy of the solution.

We have focused our effort on analysing the uniqueness of the solution. Our findings claim that the models can be univocally inverted when the search of optimal solution is narrowed by defining the physical mechanism and the source geometry. Due to the limited amount of observation points available in real cases, we have studied how the accuracy is affected by the number of measuring points. Naturally, not only the number of observations but also their distribution on the ground surface plays a role on constraining the solution. Moreover, the capability of narrowing the solution is strongly dependent on the source size with respect to the spatial extent of observations. A rough estimation of the density of measuring points, required to well constrain the solution, was given. It was shown that magnetic anomalies generated by a Mogi source, independently of the geophysical mechanism, are unambiguously inverted even with a measuring array consisting of a few points (larger than 2×2). For Okada sources, the fault location and the orientation are estimated with high accuracy, while a subset of parameters, consisting of width, length, dip and dislocation, exhibit an error ranging between 5 and 35 per cent. Techniques for avoiding this problem were investigated. The GAs setting parameters (population number, number of generations, crossover and mutation probability, etc.) were better tuned to improve the accuracy of the solution. A too large population size may waste computational resources, without further improving the convergence of the algorithm versus the optimal solution. To overcome this difficulty and save computation time, a two-step procedure is proposed by reducing the dimensionality of the space parameters once promising areas in the solution space have been discovered.

Both synthetic and real case examples proved that GA technique was especially suitable for taking into account the non-linearity involved in the inversion of the volcanomagnetic anomalies. Starting from these results, the next step would be to adapt the GAs for

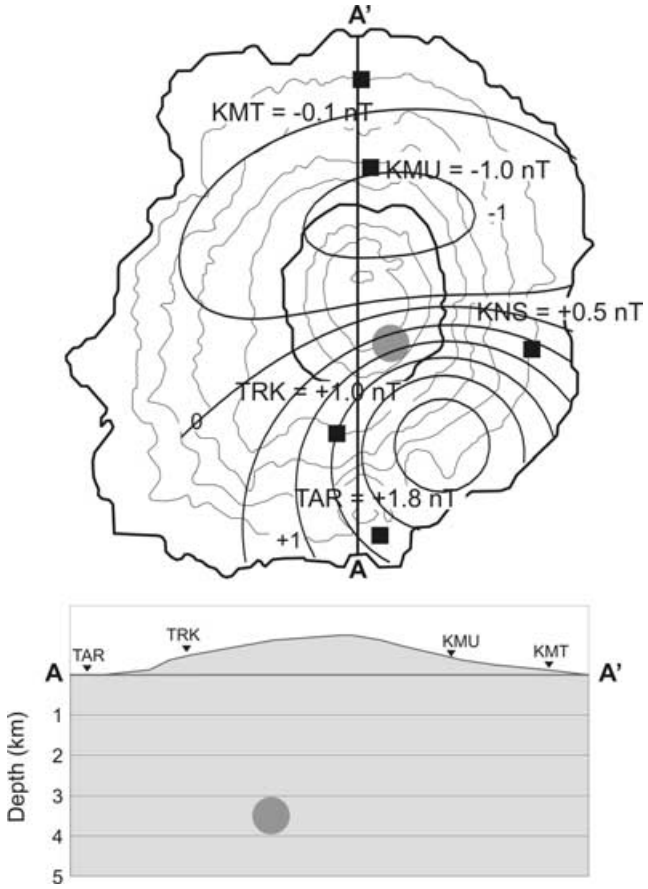

Figure 13. The magnetic monitoring array at Miyakejima volcano (after Sasai *et al.* 2002). The five stations are those used for the GA inversion. The computed anomaly and the amplitude of the step-like magnetic variations recorded in correspondence with the July 14 tilt-step event are also reported.

inverting more sources simultaneously. It involves searching for a higher number of parameters. In such a case, the inversion procedure could suffer from ill-posed problems. To make the problem well posed, it would be necessary to specify other constraints on the feasible set by considering additional geophysical data. Hence, the high number of parameters to be identified could entail the need for integrated inversion of geophysical parameters (e.g. ground deformation and gravimetric data), which independently reflect the state of volcano. Hence, further works would include attempts to model magnetic, gravity and ground deformation data simultaneously in order to provide better constraints on the solutions.

ACKNOWLEDGMENTS

This work was developed in the frame of the TecnoLab, the laboratory for the technological advance in geophysics organized by DIEES-UNICT and INGV-CT. We are grateful to reviewers for constructive and helpful comments that improved greatly the manuscript. This research was supported by project EPOT of the Gruppo Nazionale per la Vulcanologia of the INGV.

REFERENCES

Bhattacharyya, B.K., 1964. Magnetic anomalies due to prism-shaped bodies with arbitrary polarization, *Geophysics,* **29,** n.4 517–533.

Blakely, R.J., 1995. *Potential theory in gravity and magnetic applications,* Cambridge University Press, New York, pp. 435.

Del Negro, C. & Ferrucci, F., 1998. Magnetic history of a dyke on Mount Etna (Sicily), *Geophys. J. Int.,* **133,** 451–458.

Del Negro, C. & Currenti, G., 2003. Volcanomagnetic signals associated with the 2001 flank eruption of Mt. Etna (Italy), *Geophys. Res. Lett.,* **30**(7), 1357, doi:10.1029/2002GL015481.

Del Negro, C. & Nunnari, G., 2003. A Software Tool for Modelling Volcanomagnetic Data, *Proc. of the International Association for Mathematica Geology, IAMG 2003,* Portsmouth, UK.

Del Negro, C., Currenti, G., Napoli, R. & Vicari, A., 2004. Volcanomagnetic Changes Accompanying the Onset of the 2002–2003. Eruption of Mt. Etna (Italy), accepted to *Earth planet. Sci. Lett.,* **229,** 1–14.

Edwards, R.N., 1974. The magnetometric resistivity method and its application to the mapping of a fault, *Can. J. Earth. Sci.,* **11,** 1136–1156.

Fenoglio, M.A., Johnston, M.J.S., Byerlee, J.D., 1995. Magnetic and electric fields associated with changes in high pore pressure in fault zones: application to the Loma Prieta ULF emissions, *J. Geophys. Res.,* **100**(B7), 12 951–12 958.

Fitterman, D.V., 1978. Electrokinetic and magnetic anomalies associated with dilatent regions in a layered earth, *J. Geophys. Res.,* **83,** 5923–5928.

Fitterman, D.V., 1979. Theory of electrokinetic-magnetic anomalies in a faulted half-space, *J. Geophys. Res.,* **84,** 6031–6040.

Fitterman, D.V., 1981. Correction to theory of electrokinetic magnetic anomalies in a faulted half space, *J. Geophys. Res.,* **86,** 9585–9588.

Goldberg, D.E., 1989. *Genetic algorithms in search, optimization, and machine learning*. Reading, MA, Addison-Wesley.

Hagiwara, Y., 1977. The Mogi model as a possible cause of the crustal uplift in the eastern part of Izu Peninsula and the related gravity change, *Bull. Earthquake Res. Inst. Univ. Tokyo,* **52,** 301–309.

Hamano, Y. *et al.*, 1990. Geomagnetic Variations Observed after the 1986 Eruption of Izu-Oshima Volcano, *J. Geomagn. Geoelectr.,* **42,** 319–336.

Holland J.H., 1975. *Adaptation in natural and artificial system,* University of Michigan Press, Ann Arbor, MI.

Ishido, T. & Mizutani, H., 1981. Experimental and theoretical basis of electrokinetic phenomena in rock-water systems and its applications to geophysics, *J. Geophys. Res.,* **6,** 1763–1775.

Johnston M.J.S., 1989. Review of magnetic and electric field effects near active faults and volcanoes in the U.S.A., *Earth Planet Sci. Lett.,* **57,** 47–63.

Jousset, P., Mori, H. & Okada, H., 2003. Elastic models for the magma intrusion associated with the 2000 eruption of Usu Volcano, Hokkaido, Japan, *J. Volcan. Geotherm. Res.,* **2607,** 1–26.

Lavrentiev, M.M., Avdeev, A.V., Lavrentiev, M.M. & Priimenko, V.I., 2003. *Inverse Problems of Mathematical Physics,* VSP Publ., The Netherlands, p. 276.

Michalewicz, Z., 1992. *Genetic Alogorithms+Data Structures=Evolution Programs*. Springer, New York, NY.

Murakami H., 1989. Geomagnetic fields produced by electrokinetic sources, *J. Geomagn. Geoelectr.,* **41,** 221–247.

Nourbehecht, B., 1963. Irreversible thermodynamic effects in inhomogeneous media and their applications in certain geoelectric problems, *Thesis*, Massachussets Institute of Technology, Cambridge, Massachussets.

Nunnari, G., Bertucco, L. & Ferrucci, F., 2001. A Neural Approach to the Integrated Inversion of Geophisical Data Types, *IEEE Transaction on Geosciences and Remote Sensing,* **39**(4), 736–748.

Parkinson, W.D., 1983. *Introduction to geomagnetism,* Scottish Academic Press, Edinburgh.

Ramillien, G., 2001. Genetic algorithms for geophysical parameter inversion from altimeter data, *Geophys. J. Int.,* **147,** 393–402.

Rikitake, T., 1952. On magnetization of volcanoes, *Bull. Earthq. Res. Inst.,* University of Tokio **30,** 71–82.

Rikitake, T. & Yokoyama, I., 1955. Volcanic activity and changes in geomagnetism, *J. Geophys. Res.,* **60,** 165–172.

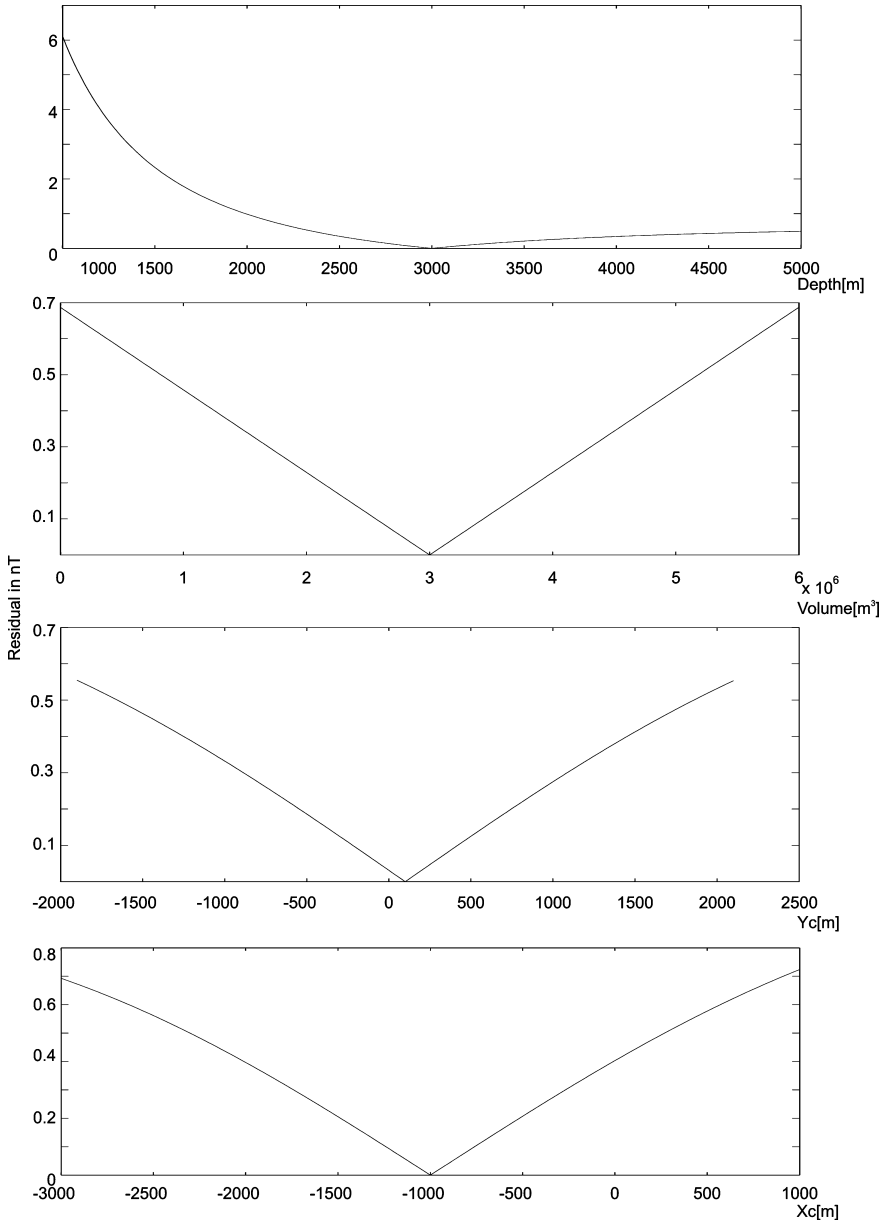

Figure 14. Sensitivity of fit for the piezomagnetic Mogi model solution obtained for the Miyakejima case study.

Russo, G., Gilberti, G. & Sartoris, G., 1997. Numerical modelling of surface deformation and mechanical stability of Vesuvius volcano, Italy, *J. Geophys. Res.,* **102,** 24 785–24 800.

Sasai, Y., 1980. Application of the elasticity theory of dislocations to tectonomagnetic modelling, *Bull. of the Earthquake Research Institute,* **55,** 387–447.

Sasai, Y., 1991a. Piezomagnetic field associated with the Mogi model revisited: analytical solution for finite spherical source, . *J. Geomagn. Geoelectr.,* **43,** 21–64.

Sasai, Y., 1991b. Tectonomagnetic modelling on the basis of the linear piezomagnetic effect, *Bull. Earthq. Res. Inst., Univ. Tokyo,* **66,** 585–722.

Sasai, Y., Uyeshima, M., Zlotnicki, J., Utada, H., Kagiyama, T., Hashimoto, T. & Takahashi, Y., 2002. Magnetic and electric field observations during the 2000 activity of Miyake-jima volcano, Central Japan, *Earth planet. Sci. Lett.,* **203,** 769–777.

Stacey, F.D., 1964. The seismomagnetic effect, *Pure and Applied Geophysics.,* **58,** 5–22.

Stacey, F.D. & Banerjee, S.K., 1974. *The physical principles of rock magnetism,* Elsevier, Amsterdam.

Stacey, F.D., Barr, K.G. & Robson G.R., 1965. The volcanomagnetic effect, *Pageoph,* **62,** 96–104.

Talwani, M., 1965. Computation with the help of a digital computer of magnetic anomalies caused by bodies of arbitrary shape, *Geophysics,* **30,** 797–817.

Tanaka, A., Okubo, Y. & Matsubayashi, O., 1999. Curie point depth based on spectrum analysis of the magnetic anomaly data in East and Southeast Asia, *Tectonophysics,* **306,** 461–470.

Tiampo, K.F., Rundle, J.B., Fernandez, J. & Langbein, J.O., 2000. Spherical and ellipsoidal volcanic sources at Long Valley caldera, California, using a genetic algorithm inversion technique, *J. Volcan. Geotherm. Res.,* **102,** 189–206.

Tiampo, K.F., Fernandez, J., Jentzschc, G., Charco, M. & Rundle, J.B., 2004a. Volcanic source inversion using a genetic algorithm and an elastic-gravitational layered earth model for magmatic intrusions, *Computers and Geosciences,* **30,** 985–1001.

Tiampo, K.F., Fernandez, J., Jentzsch, G., Charco, M. & Rundle, J.B., 2004b. New results at Mayon, Philippines, from a joint of gravity and deformation measurements, *Pure appl. Geophys*. **161,** 1433–1452.

Ukawa, M., Fujita, E., Yamamoto, E., Okada, Y. & Kikuchi, M., 2000. The 2000 Miyakejima eruption: crustal deformation and earthquakes observed by the NIED Miyakejima observation network, *Earth Planets Space,* **52**(8), pp. xix–xxvi.

Utsugi, M., Nishida, Y. & Sasai, Y., 2000. Piezomagnetic potentials due to an inclinated rectangular fault in a semi-infinite medium, *Geophys. J. Int.* **140,** 479–492.

Zlotnicki, J. & Bof, M., 1998. Volcanomagnetic signals associated with the quasi-continuous activity of the andesitic Merapi volcano, Inodonesia: 1990–1995, *Physics of the Earth and Planetary Interiors,* **105,** 119–130.

Zlotnicki, J. & Le Mouel, J.L., 1988. Volcanomagnetic effects observed on Piton de la Fournaise Volcano (Reunion Island): 1985–1987, *J. Geophys. Res.,* **93,** 9157–9171.